AD-A043 779   HARRY DIAMOND LABS   ADELPHI MD   F/G 9/5
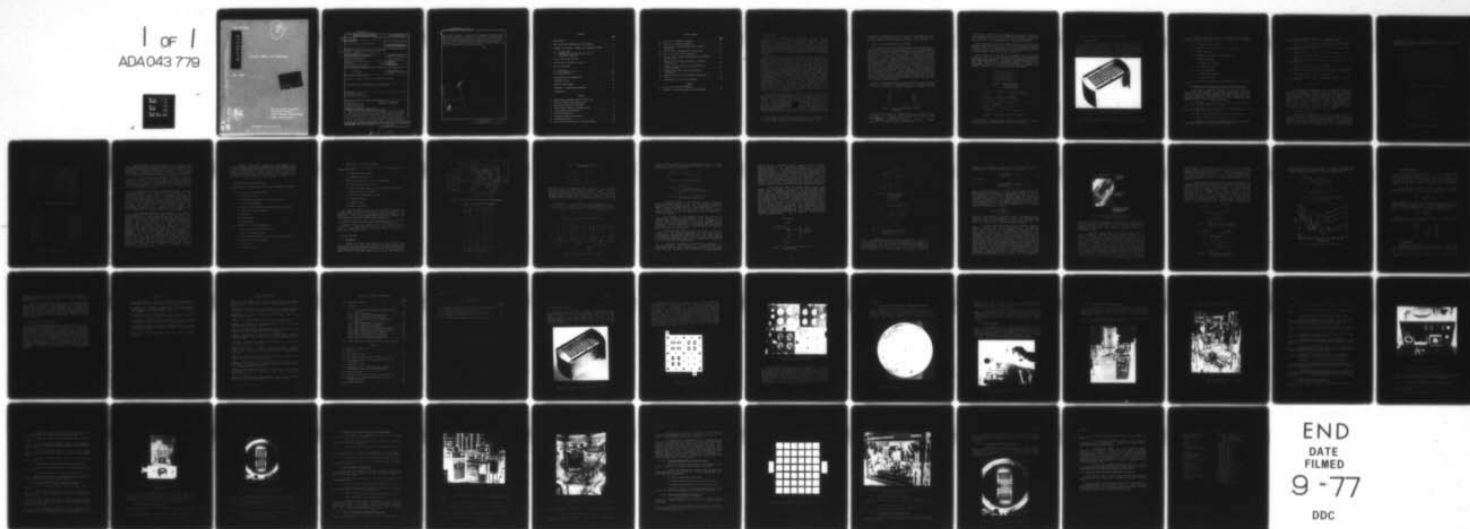   ACOUSTIC DELAY LINE FABRICATION.(U)
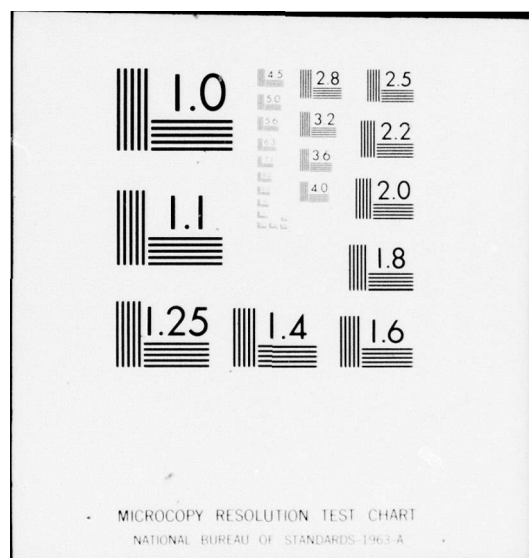   JUL 77   S I LIEBERMAN, O L MEYER

UNCLASSIFIED   HDL-TR-1820   NL
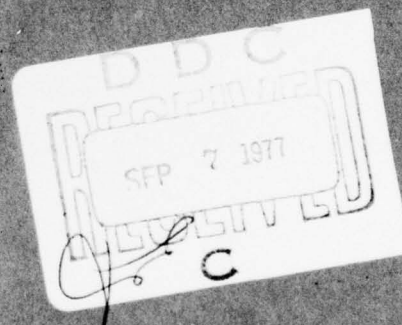
1 OF 1
ADA 043 779

END
DATE
FILMED
9-77
DDC

MICROCOPY RESOLUTION TEST CHART
NATIONAL BUREAU OF STANDARDS-1963-A

HDL-TR-1820

Acoustic Delay Line Fabrication

July 1977

SECURITY CLASSIFICATION OF THIS PAGE *(When Data Entered)*

REPORT DOCUMENTATION PAGE		READ INSTRUCTIONS BEFORE COMPLETING FORM
1. REPORT NUMBER HDL-TR-1820	2. GOVT ACCESSION NO.	3. RECIPIENT'S CATALOG NUMBER
4. TITLE *(and Subtitle)* Acoustic Delay Line Fabrication.		5. TYPE OF REPORT & PERIOD COVERED Technical Report.
		6. PERFORMING ORG. REPORT NUMBER
7. AUTHOR(s) Martin J. Reddan, Theodore V. Blomquist Stuart I. Lieberman, John H. Wasilik Owen L. Meyer		8. CONTRACT OR GRANT NUMBER(s)
9. PERFORMING ORGANIZATION NAME AND ADDRESS Harry Diamond Laboratories 2800 Powder Mill Road Adelphi, MD 20783		10. PROGRAM ELEMENT, PROJECT, TASK AREA & WORK UNIT NUMBERS PRON: 815A178801M1A9 Program element: P
11. CONTROLLING OFFICE NAME AND ADDRESS Commander U.S. Army Armament Command Rock Island, IL 61201		12. REPORT DATE July 1977
		13. NUMBER OF PAGES 51
14. MONITORING AGENCY NAME & ADDRESS*(if different from Controlling Office)*		15. SECURITY CLASS. *(of this report)* UNCLASSIFIED
		15a. DECLASSIFICATION/DOWNGRADING SCHEDULE

16. DISTRIBUTION STATEMENT *(of this Report)*

Approved for public release; distribution unlimited.

17. DISTRIBUTION STATEMENT *(of the abstract entered in Block 20, if different from Report)*

18. SUPPLEMENTARY NOTES

HDL Project: 367535
DRCMS Code: 4932.05.3061

19. KEY WORDS *(Continue on reverse side if necessary and identify by block number)*

Delay line
Acoustic delay line
Microwave acoustics
Matched delay lines
Microwave ultrasonic delay lines

Sputtered transducers
Computer-aided design

20. ABSTRACT *(Continue on reverse side if necessary and identify by block number)*

This report describes work performed at the Harry Diamond Laboratories to establish a viable production method for fabricating series-transducer delay lines. The devices considered in this report consist of a crystal delay medium with a series-connected matrix of zinc oxide transducers deposited on each end. This is a new concept (U.S. Patent 3,893,048) which eliminates the need for external electrical matching. Two basic fabrication approaches were tried successfully, and a combination of the two

DD $_{1\ JAN\ 73}^{FORM}$ **1473** EDITION OF 1 NOV 65 IS OBSOLETE

1   UNCLASSIFIED

was finally adopted.   A step-by-step processing section furnishes
complete data regarding the materials, methods, and techniques
employed, with sufficient detail to facilitate technology trans-
fer.   The devices fabricated operated typically in the bulk wave
mode in the 3- to 4-GHz range and displayed through insertion
losses of 30 to 50 dB for delays in the 0.5-ms region.   Some life-
time and ruggedness data also are included.

CONTENTS

FIGURES

3

FIGURES (CONT'D)

1. INTRODUCTION

This report describes work performed at the Harry Diamond Laboratories (HDL) to establish fabrication techniques for the production of series-transducer acoustic delay lines. The work was supported by the U.S. Army Armament Command as a Materials, Methods, and Techniques Effort (MM&TE), Project AMC 5753061, APA 4932, with the title "Series Array Acoustic Delay Line Fabrication." Appendix A furnishes a detailed account of the materials and processes used during the course of the program and gives a step-by-step explanation of the fabrication techniques.

Important applications exist for devices which provide an exact amount of delay for electrical signals. For these applications, acoustic techniques provide low-cost, gun-rugged delay devices which have replaced bulky transmission lines. Some applications include electronic fuzing, target simulation, radar calibrators, and electronic countermeasures. For the past several years, the need has been satisfied by devices which utilize piezoelectric thin films placed on suitable crystalline substrates in rod form. The form of the device to be considered in this report consists of a crystal delay medium with thin-film piezoelectric transducers and matching networks ruggedly integrated onto each end of the crystal. The first transducer converts an electromagnetic signal into a microacoustic wave which propagates through the crystal at the speed of sound (10^4 times slower than the electromagnetic waves). The signal is then reconverted into an electromagnetic signal by the transducer on the other end, and it emerges with a time delay proportional to the crystal length. Such devices furnish a low-loss, very compact delay device in the submicrosecond region, several orders of magnitude smaller than the size and weight required for transmission lines.

The project had as its principal purpose the solution of production problems which were responsible for the relatively high cost of bulk-wave devices. Prior to commencement of this project, the necessary research and development had been completed on a new approach to the critical problem of achieving an electrical match with the delay line. Up to this point, extensive work had been performed on piezoelectric, bulk-wave transducers operating at   wave frequencies.* In 1973, a new concept was developed at HDL   eliminated the tedious and costly matching processes used at that time by others. Crucial support was found in a publication by Weinert and de Klerk[1] which showed that each

---

[1]R. W. Weinert and J. de Klerk, A Thin-Film Mosaic Transducer for Bulk Waves, IEEE Trans. Sonics Ultrason., SU-19 (July 1972), 354.

*For background literature, see the Selected Bibliography.

transducer is independent and that the acoustic beam generated by each transducer does not interfere with its neighbor. The MM&TE goals were set up to refine the manufacturing processes for this new concept.

2. DELAY LINE AND CONVENTIONAL DEVICE COMPARED

The configuration of a typical bulk microwave acoustic delay line is shown in figure 1. Matching loss is present due to the difficulty in achieving a good match between the transducer input impedance and the input signal. Tuned insertion loss depends strongly upon the tuning network employed and upon contact losses. In the past, the required matching to a 50-ohm line was accomplished by a variety of techniques, all of which failed to meet one important criterion--small size. For example, a quarter-wave transformer is about 1 in. (2.54 cm) at 2.0 GHz, which means that the matching section far exceeds the usual length of the delay medium. A two-element network was described[2] in 1969 that used lumped circuit elements and required only a fraction of the space needed by the transformer approach. However, it was still external to the delay medium and demanded tedious adjustment during manufacture, which increased the cost. A novel solution developed at HDL[3] provided that the matching circuit be placed on the end of the rod itself. This proved to require very high precision during fabrication, including close control of piezoelectric film thickness and exact dimensioning of thin, metallic-stripe inductances.

Finally, a breakthrough design was originated at HDL which achieved matching to a 50-ohm line by depositing an array of single transducers in series and placing a suitable inductance in series with the
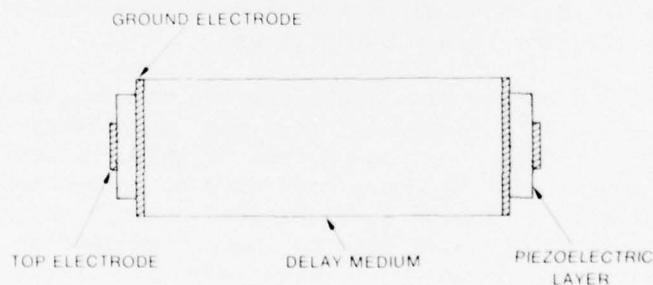

Figure 1. Typical bulk microwave acoustic delay line.

---

[2]T. Reeder and D. Winslow, *Characteristics of Microwave Acoustic Transducers for Volume Wave Excitation*, IEEE Trans. Microwave Theory Tech., *MMT-17*, No. 11 (November 1969), 932.

[3]S. Lieberman, *Matched Delay Lines with Solderable Transducer Electrodes*, U.S. Patent 3,688,222 (29 August 1972).

combination. The number of single transducers introduced into the array and the inductances required were determined from previous knowledge of the parameters of a single transducer. The configuration adopted is shown in figure 2, as delineated by the ground electrode pattern.

Delay lines were fabricated to this design, and they proved to be remarkably broadband (nearly 1 octave at 3 GHz) and to have acceptable insertion loss. Since the necessary research and development had been recently completed, the production of this device became the subject of the present MM&TE, which was initiated in August 1973.

An equivalent circuit for a delay-line transducer can be represented as shown in figure 3. As can be seen by inspection, the circuit models each layer of the transducer as an acoustic transmission line with its own characteristic impedance. The various individual components of the model were combined,[4] and the resulting equations were solved on a programmable calculator. A listing of the program is available upon request. Lieberman details the model, program, and process.

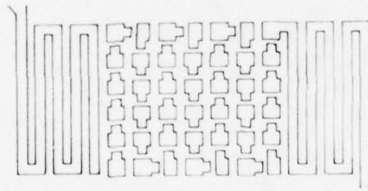Figure 2.   Mask for ground-
layer metalliza-
tion (early model).
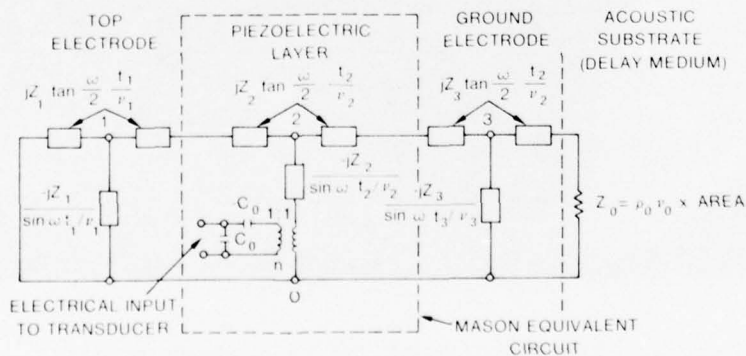
Figure 3.   Equivalent circuit for transducer.

[4]S. Lieberman, A Rugged Microwave Acoustic Delay Line with Integral Matching, Harry Diamond Laboratories TR-1738 (February 1976).

3. PROGRESS ON MATERIALS, METHODS, AND TECHNIQUES EFFORT

3.1 Initial Steps

The first goal in time phasing this project was the fabrication
of engineering samples, scheduled to start in January 1974.   In
preparation for this step, it was necessary to finalize the prototype.
The design adopted is shown in figure 4. Groups of engineering samples
were then fabricated. These were made by using a set of masks specially
designed for this purpose and used in conjunction with a positive
photoresist. Good performance was obtained from these units.[5]
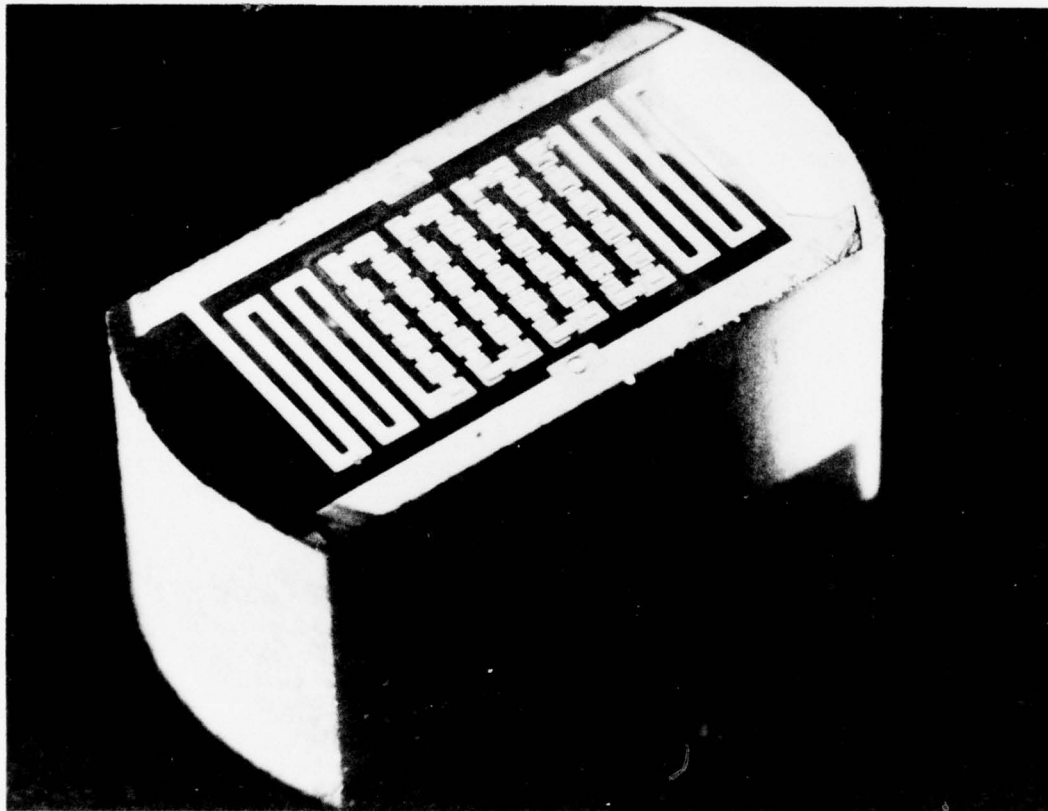
413-75

Figure 4. Final design of series transducer array.

---

[5]S. Lieberman, A Matched MIC Delay Line Transducer Using a Series
Array, Proc. 1974 IEEE International Solid-State Circuits Conference
(1974), 100-101, 235.

From the experience gained in producing the engineering samples, a number of important conclusions were drawn, and the critical processing parameters were identified:

    a. Rod cleaning and preparation

    b. Masking techniques, including correct registry

    c. Resist techniques

    d. Substrate metallization (ground electrode)

        (1) Metal to be used

        (2) Temperature of substrate

        (3) Thickness control

    e. Zinc oxide deposition

        (1) Sputtering parameters

        (2) Thickness monitor

    f. Top layer metallization (same parameters as for ground electrode)

3.2 Commentary on Each Identified Critical Processing Parameter

Rod cleaning is extremely important, and an effective method was evolved which included special cleaning fixtures. These are individual hollow Pyrex glass spheres having several small holes in the surface. By means of an attached handle, the sphere is lowered into the cleaning solution after it is loaded with a rod. Cleaning is done immediately prior to use. The steps are these:

    a. Degrease the sphere and rod with Freon, trichloroethylene, and acetone, scrub gently with a cotton swab.

    b. Soak for 1 hr in a hot acid of three parts H_2SO_4, one part H_2O_2, and one part distilled water.

    c. Rinse in running distilled water for several minutes.

    d. Soak in distilled water until ready for use.

    e. Before use, blow with dry nitrogen and insert rods into the evaporation fixture. Use clean tweezers for handling.

The rod material chosen was crystalline quartz, Z-cut (longitudinal propagation). These are the rod specifications:

Material: Z-cut (longitudinal propagation) crystalline quartz

Orientation: Angle between rod axis and optic axis not to exceed ±30 min (±1/2 deg)

Diameter of rod: 0.250, +0, -0.002 in. (0.635, +0, -0.005 cm)

Length of rod: 0.124 ± 0.002 in. (0.315 ± 0.005 cm)

Parallelism of end faces: Best effort to achieve 15 to 20 s, not to exceed 30 s

Flatness of end faces: 1/10 wavelength

Surface finish: Must meet specification of 20-5 or better (no blemish can exceed 0.020 in. (0.05 cm) long or 0.0005 in. (0.0013 cm) deep)

Ends perpendicular to body: 20 min or less

End bevel: Slight bevel, approximately 0.005 in. (0.013 cm) long, as shown:

bevel

The foregoing are comparable to the standards needed for laser work and are obtainable from several commercial sources. Experience showed that best transducers were associated with high optical polish on the end faces of the rods. End-face parallelism is important, as well as the crystalline orientation in respect to the rod axis. As an example of the effect of misalignment between the rod axis and the crystal axis, a simple calculation shows that a misalignment of 43 s at the sending transducer causes the acoustic beam generated on one side of the delay line rod to miss about 50 percent of the area of the opposite receiving transducer, for a transducer 0.010 in. (0.0254 cm) on a side and a rod 0.4 in. (1.016 cm) long.

4. TYPICAL METAL MASK APPROACH

Masking with photoresist led to the concept that it would be desirable to have an alternative process to the wet-chemical procedures used with photoresist. The first masks were made by cutting patterns on rubylith. These were photographed and reduced in size, and the resulting patterns were transferred to glass plates. A modified mask process was next adopted. Line drawings for the desired pattern were

prepared and furnished to the Buckbee-Mears Co., St. Paul, MN, for processing. That company produced a set of metal evaporation masks shown in figures 5 to 8.
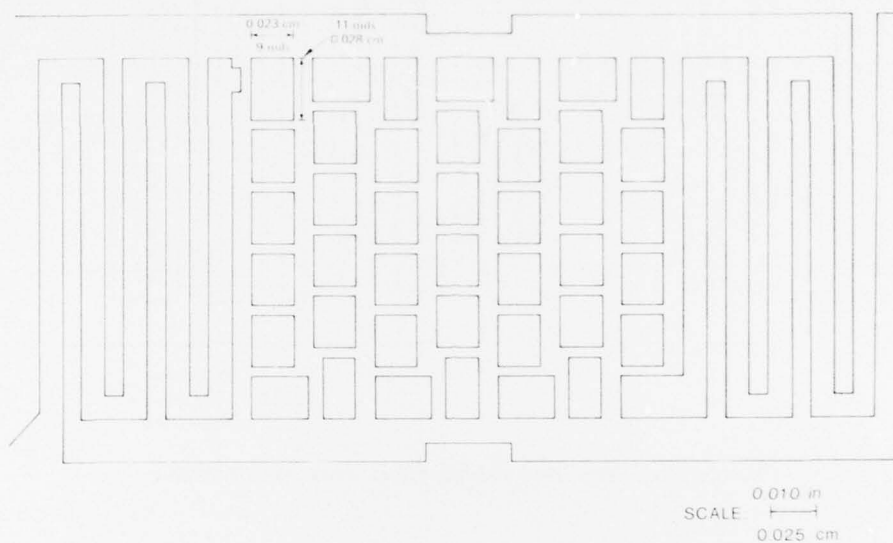

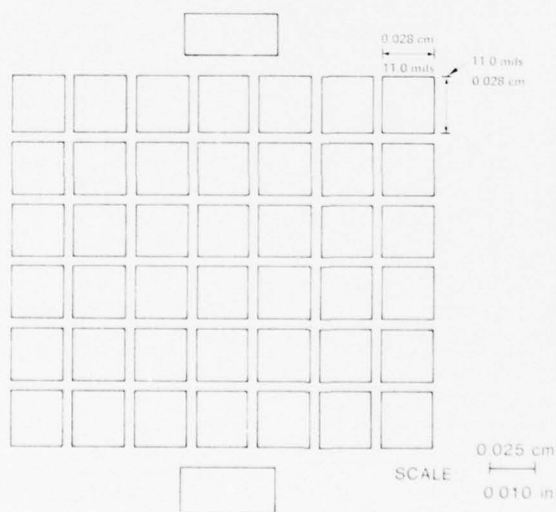Figure 5. Ground pattern metallization.
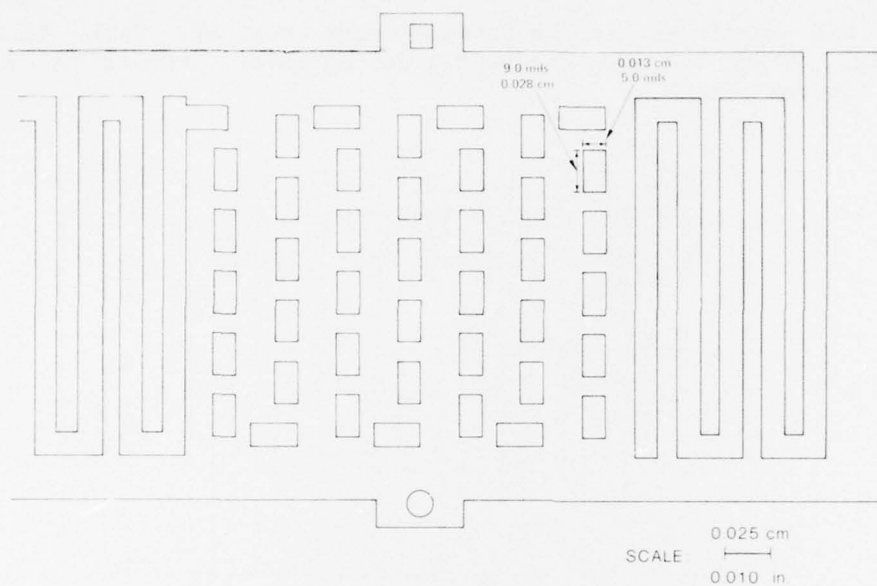

Figure 6. Zinc oxide deposition.

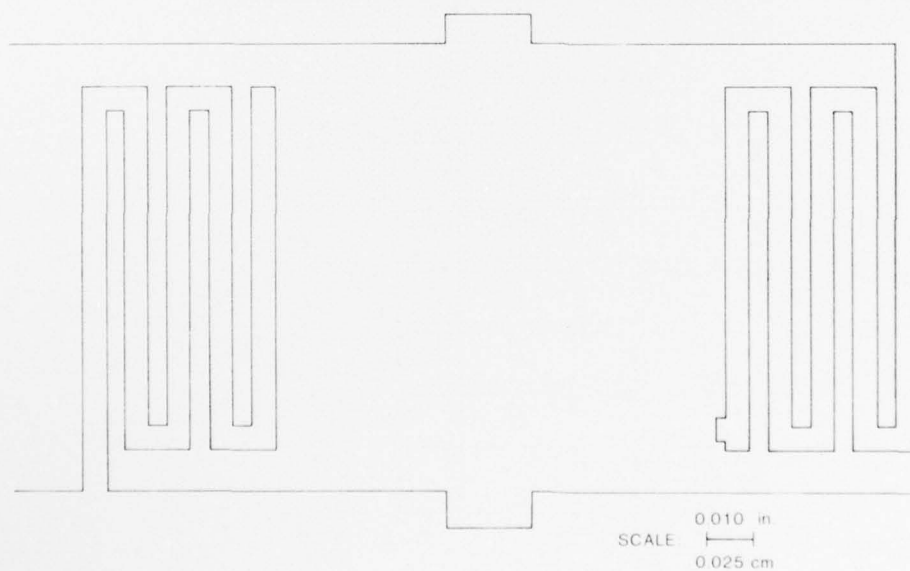Figure 7. Top metallization and inductors.

Figure 8. Thickened inductors.

12

Resist techniques used for delineation of patterns were adopted from standard semiconductor processes. Material most frequently used was Shipley positive resist AZ-1350, applied by using a spinner rotating at 6000 rpm. One drop was applied within the first 5 s. Each side was done separately, followed by a 5-min bake at 70°C and then a final bake of 15 min. Units were then stored in a clean, covered aluminum dish.

For substrate metallization-ground electrodes, initially, chromium was used (a thin layer of about 20 to 30 nm) deposited by evaporation. The substrate was held at approximately 200°C. A layer of gold (70 nm) was then put on by evaporation. For each deposition, the thickness was monitored by a Sloan thickness monitor (frequency shifts due to mass loading of the crystal).

Titanium also was used for substrate metallization. This metal is strongly recommended by certain laboratories because (1) it has scavenging properties which produce a cleaner substrate and, consequently, better adherence; and (2) it encourages the gold layer to grow with the proper orientation (111), upon which subsequent sputtered ZnO epitaxial growth results in an ordered layer for good transducer action. A very thin film (20 to 30 nm) was laid down by a flash method. A common technique used titanium wire cut into small lengths (a few millimeters) and placed in a conical tungsten heater. Some inconvenience resulted from the tendency for a titanium-tungsten alloy to form, which led to early failure of the conical heater.

Zinc oxide was deposited by rf sputtering. Zinc oxide is strongly piezoelectric and has been deposited as a thin film for many applications where an electromechanical transducer is required. X-ray analysis showed that the film consisted of many very small crystallites with the c-axis normal or slightly tilted from normal to the substrate surface. (ZnO in crystalline form is a wurtzite structure with hexagonal symmetry when viewed along the c-axis.) The rf field was applied normal to the film itself and parallel to the c-axis. Deposition was accomplished with a mixture 80 percent of argon and 20 percent of oxygen. A substrate heater was used to establish a temperature of 100°C before sputtering began. During sputtering, additional heat from the discharge raised the temperature to approximately 120°C, where it remained steady throughout the deposition process. An rf power input was set at 300 W. Gas pressure was set at 14 μm, and a dark space of about 1/2 in. (1.27 cm) was maintained. A typical sputtering rate of 170 a.u./min yielded good results. Sputtering rates were continuously monitored by an Inficon controller (mass-loaded crystal). A typical ZnO thickness of 3000 a.u. ± 10 percent was deposited.

Top layer metallization followed the same procedures as for ground electrodes and employed the same materials and equipment. Either titanium or chromium was used with equal effectiveness. Chromium was slightly favored because of a greater ease of handling (less of a tendency to alloy with the tungsten heater) and a lower melting temperature (1450° versus 1850°C). The thickness was chromium--200 a.u., gold--700 a.u. (as for ground layer metallization).

5. TYPICAL PHOTOLITHOGRAPHIC APPROACH

The processing steps described below are performed on both ends of the rod.

a. Step one: Put on ground pattern

(1) Clean four rods.

(2) Evaporate chromium-gold over entire end of rod.

(3) Coat with photoresist.

(4) Mount rod and photomask in hand-held alignment fixture.

(5) Expose and develop photomask.

(6) Etch gold.

(7) Etch chromium.

(8) Remove resist.

b. Step two: Put on ZnO transducers.

(1) Sputter ZnO over entire end of rod.

(2) Coat rod with photoresist.

(3) Mount rod and photomask in microscope alignment fixture.

(4) Expose and develop photomask.

(5) Etch ZnO.

(6) Remove photoresist.

c.   Step three: Put on top electrodes.

(1) Microscopically, align metal mask on rod and mount it in evaporation system.

(2) Evaporate chromium layer.

(3) Evaporate gold layer.

d.   Alternative step three: Put on top electrodes.

(1) Coat with photoresist overall.

(2) Mount rod and photomask in microscope alignment fixture.

(3) Expose and develop photomask.

(4) Mount rods in evaporation system.

(5) Evaporate chromium.

(6) Evaporate gold.

(7) Remove photoresist.

Use of this alternative step has been limited by low yields due to poor adhesion of the top electrodes. The trouble is thought to be associated with the effect of relatively high temperatures on the photoresist.   There is some unavoidable exposure to transient high temperature from the heater filament during evaporation.

A third and final approach, a hybrid of the two above, as described in appendix A, appears to be the most successful method thus far.

Electrical testing was conducted with the arrangement shown in figure 9 (p 16).   Typical results are shown in table I (p 16).   Table II (p 17) is a summary of the design values of transducer parameters in common with all computer runs.

6.   SPECIAL CARE AREAS

6.1 Discussion

Because the metal masks could not be made thicker than 0.001 in. (0.0025 cm), extra care was taken when a metal mask was used in performing the top electrode metallization. The mask must be kept in close contact with the substrate; this was done by using snap rings. Any warpage or lifting of the mask permits metal or ZnO to diffuse under the
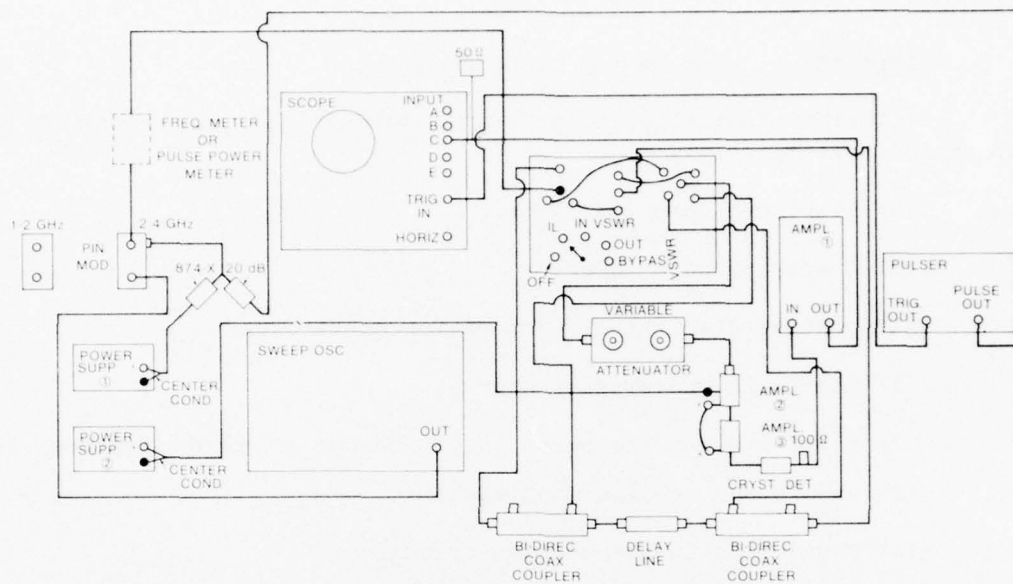
Figure 9.   Test position for insertion loss measurements.

TABLE I.   TYPICAL ELECTRICAL PERFORMANCE[a]

Rod	Frequency (GHz)	Through loss (dB)	Reflection loss (dB)	
			Side 1	Side 2
DF-5	3.05	32	44	52
	3.26	39	48	54
	3.42	44	54	46.5
DH-5	3.14	33	47	39
	3.41	44	57	47
FF	3.32	47	48	38
	3.5	49	49	38
FG	3.5	41	49	48
FH	3.5	52	56	45
FI	3.5	44	56	51
	3.5	41.5	53.5[b]	50.5[b]
FR	2.97	25	43	38
	3.21	32	43	43
	3.43	38	49	46.5
FT	3.42	36	45	50
	3.5	38.5	48.5	51
FX	2.98	49.5	66.5	45
	3.43	59	69	51
FY	3.15	38.5	50	54.5
	3.5	49.5	64	63

[a]All data were taken without external tuning.
[b]After removal of parasitic Au on side of rod.

TABLE II. SUMMARY OF SERIES TRANSDUCER
DESIGN PARAMETERS

Parameter	Data
Ground electrode thickness	0.09 μm
ZnO thickness	0.38 μm
Top electrode thickness	0.09 μm
Coupling constant	0.15
Number of transducers	42
Transducer length, width	0.005 in. (0.013 cm)
Series inductance	25.4 nH

mask edges and thus creates problems with continuity.   As an example,
figure 10 illustrates a side view of the transducer geometry. It can be
seen that if ZnO is permitted to deposit beyond the 0.002-in. (0.005-cm)
separation between ground electrodes and to cover a portion of the
adjacent ground electrode, then a high series resistance or capacitance
is added. This is seen also in the top view shown in figure 11. A high
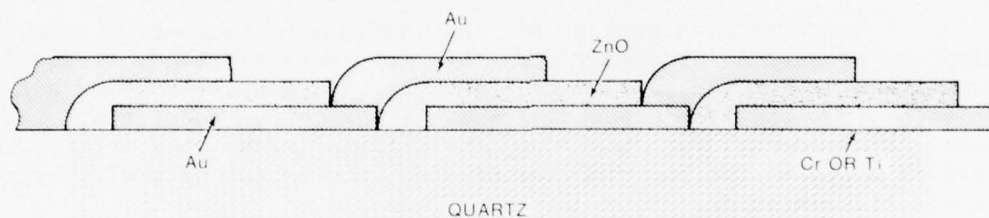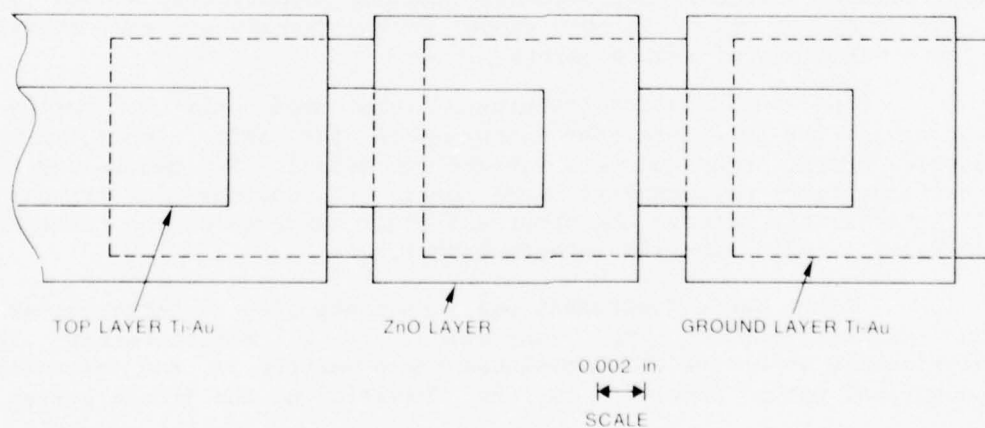

Figure 10. Side view of transducer geometry.

Figure 11. Top view of transducer geometry.

series resistance increases the loss uniformly with frequency. Series capacitance, however, detunes the overall transducer circuit, as shown by computer simulation in figure 12.

NOTES: (1) CURVE 1 TUNED LOSS
(2) CURVE 2 DETUNED LOSS FROM CONTACT
C = 27.3 pF RESULTING IN SERIES CAPACITANCE =
42 × 27.3 = 0.65 pF (ZnO THICKNESS = 18.8 nm AT
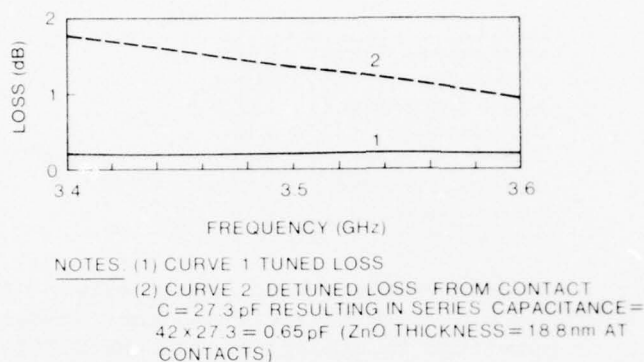CONTACTS)

Figure 12. Calculation of detuning effect
due to series capacitance.

A contrasting aspect of the diffusion problem is associated with an occasional tendency of the top metallization to develop a discontinuity at the edge of the ZnO. This is a well-known effect that sometimes results from deposition over a sharp-edge substrate. In our case, a tendency for the ZnO to diffuse under the mask causes a gradual slope at the ZnO edge, decreasing the chance of a discontinuity in the top electrode.

The topography of the deposited layers was monitored by interferometer techniques for measurement of the thickness of the component layers of the transducer. In the main, interferometry was used to measure the thicknesses of the various transducer layers. Supplementary thickness measurements included magnetically sensed stylus measurements of the surface steps of the transducer and microgram balance weighings of sample layers.

Since these latter techniques were used only to verify the accuracy of the interferometer measurements for this report, only the interferometric techniques are reviewed in detail. Two general types of interferometric measurements were used: (1) contour line fringes and (2) interference between the upper and lower surfaces of the transparent ZnO films (within-the-film interferences).

The basic instrument was a noncontacting interferometer of the Michelson-Morley type consisting of a Watson-Barnet 16-mm interference objective which replaced the objective of the microscope. The optical paths involved in the formation of the fringe system are

shown in figure 13. The fringe system is formed as follows: The input light beam is split by the half-silvered mirror; half the light is directed downward to the sample; the remainder passes through the half-silvered mirror to a totally reflecting mirror. The interference fringes are formed at the half-silvered mirror by the combination of the light reflected from the sample and the totally reflecting mirror. To obtain the desired fringe system, there are three modes of motion associated with the totally reflecting mirror--translation along the direction of the original input beam and two rotations around axes normal to this direction. The first determines the fringe existence and contrast, and the latter two determine the fringe spacing and direction.

For a metallic layer, the fringe system is always formed between the upper metallic surface and the half-silvered mirror; however, when a transparent layer (film) is involved, the fringe system can be viewed as being formed within a narrow wedge consisting of the half-silvered mirror and the sample. When monochromatic illumination is used, a dark fringe occurs every time the total (up and down) optical path changes by half a wavelength. A beveled (nonprecipitous) step in the substrate results in a closer spacing of the fringes (fig. 14). When this step in the substrate is rotated in its plane 90 deg, a fringe pattern, shown in figure 15, is obtained. The configuration shown in figure 15 (fringes crossing the substrate step at approximately a right angle) is most useful in determining step heights. The height of the step is calculated by multiplying the shift in the fringe pattern observed in crossing the step by half the wavelength of the light used to form the fringe system.
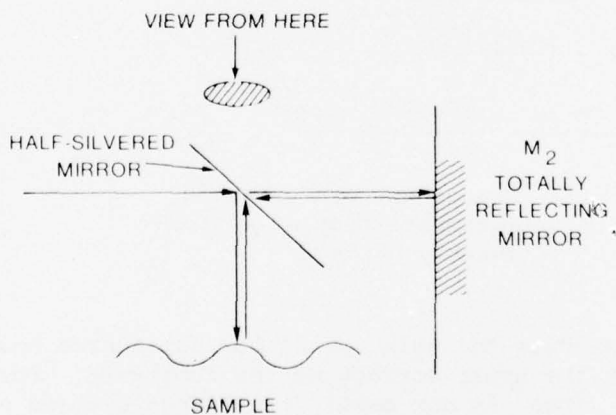

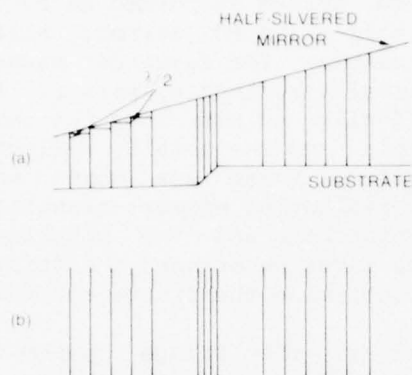Figure 13.   Optical paths in formation of
fringe system.

Figure 14.   Effect of beveled
             step in substrate:
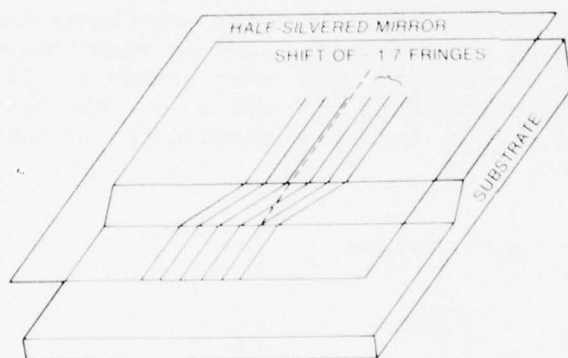   (a) side view;
             (b) top view.

Figure 15.   Fringe pattern crossing
             substrate step at approx-
             imately 90 deg.

Our analysis to this point has considered only interference fringes formed at the upper surface of the substrate. For a step in a transparent film (ZnO in our case), two fringe systems are formed, one from interference at the upper surface and a second from interference at the lower surface. The relative strengths of the two fringe systems are determined by the optical reflection coefficients of the two

20

interfaces. The reflection coefficient of the interface between two lossless dielectrics having indexes n_1 and n_2 is given by

$$R = \frac{(n_1 - n_2)^2}{(n_1 + n_2)^2} .$$ (1)

For air-ZnO,

$$R = \frac{(1.00 - 2.022)^2}{(1.00 + 2.022)^2} = 0.1144.$$

And for ZnO on Z-cut quartz, R = 0.185. Thus, for this situation, the dominant fringe system occurs at the upper surface of the ZnO. However, when gold or any other metal is the material underlying the ZnO, the high reflectivity of the ZnO-gold interface causes this interface to dominate the fringe system. It is well known that a 180-deg phase shift occurs at the boundary (interface) between a less dense and a more dense optical medium. However, at the interface between a dielectric and a metal, the situation is not so simple; the phase shift is a continuous function of the wavelength. That is,

$$\phi = \tan^{-1} \frac{2n_o k_1}{n_o^2 - n_1 - k_1^2} ,$$ (2)

where n_o is the dielectric index and $(n_1 - ik_1)$ is the complex index of the metal. Thus, for layer thicknesses of about a few wavelengths, this phase shift at the dielectric-metallic boundary must be taken into account via equation (2) for accurate thickness measurements.

A typical application of contour line fringes is shown in figure 16, which displays the structure of one of the 42 individual transducers comprising the series transducer. Steps involving only upper surface reflection are straightforward; however, in those associated with lower surface reflections, the refractive index of the transparent ZnO must be taken into account, along with the fact that the fringe shift being associated with the lower surface of the film is in the opposite direction to that of the upper surface, since here the optical path is through the transparent film. In a precipitous step in which the path of an individual fringe cannot be traced across the step being measured, white light was used to form the fringe system. Such a system consists of colored fringes with a central black fringe. From the displacement of this black fringe, the approximate number of fringe shifts upon crossing the boundary can be determined. A follow-up measurement with monochromatic light of a known wavelength then gives a more accurate determination of the step height. In our measurements, a

21

$\frac{\lambda}{2} = 0.274\ \mu m$

ZnO STEP
1.1 FRINGES
0.301 μm

ZnO SLOPING
UP HERE

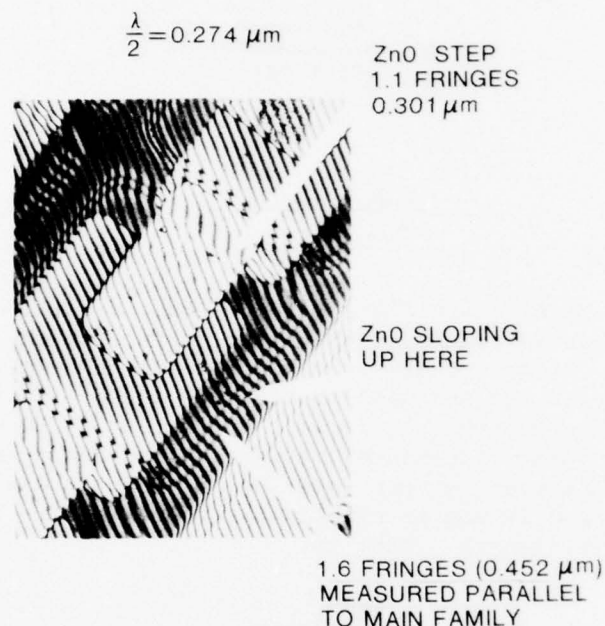1.6 FRINGES (0.452 μm)
MEASURED PARALLEL
TO MAIN FAMILY

Figure 16.   Structure of individual transducer
as shown by interferometry.

microscope illuminator was used as the light source to generate the white light fringes. Interposition of a narrow-band interference filter between this white light source and the light input tube of the interferometer was then all that was necessary to convert to monochromatic fringes.

Some other frequency effects associated with the nature of these extended-area transducer arrays merit brief consideration. One involves a stagger-tuning effect resulting from a variation in the overlap area and, thus, transducer capacitance between the ground and top electrode patterns (which has been seen on some units by visual inspection). For example, heat from the hot filament during metal evaporation can cause different relative motions of the two mask patterns on the substrate. The reversing paths of the serpentine string then result in alternating rows of larger and smaller capacitance and, thus, lower and higher frequency resonance with the series inductance. This alternation is demonstrated by computer simulation for two sets of transducers with areas 0.003 × 0.005 in. (0.008 × 0.013 cm) and 0.007 × 0.005 in. (0.018 × 0.013 cm), different from the nominal 0.005 × 0.005 in. (0.013 × 0.013 cm) of the original design (whose loss

versus frequency characteristics are shown in fig. 17). The detuning effect is shown over a wide frequency range in figure 18. Unlike *parallel*-resonant elements which yield a double peak response as in a back-to-back discriminator circuit, the *series*-resonant response shifts to a point of minimum reflection loss as a trade-off between the ideal matching requirements of a 50-ohm real part of the impedance and a zero imaginary part.

Another effect results from the capacitive coupling or feed through between the large-area input and output transducer complete with inductors and contact regions in a two-port device. This cross coupling can be viewed as the output transducer shunting the input through an effective coupling capacitance and vice versa. The change in loss characteristics with frequency for several values of coupling capacitance, about a nominal calculated value, are shown in figure 19. The effect of varying the ZnO transducer thickness and, thus, the electrical capacitance and acoustical resonance at a fixed coupling capacitance is shown in figure 20. These computer simulations are typical of the experimental results seen with the 0.5-μs delay lines
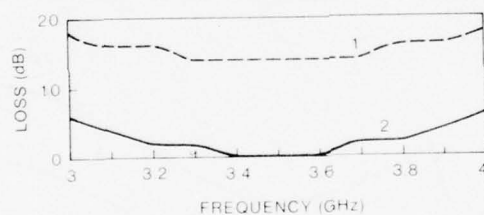
NOTES (1) CURVE 1 UNTUNED LOSS
(2) CURVE 2 TUNED LOSS
(3) SERIES R = 10 Ω

Figure 17.   Example of design variation of
insertion loss versus frequency.
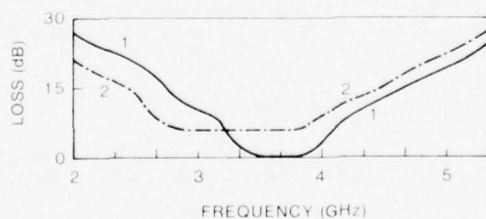
NOTES (1) CURVE 1 ALL ELEMENTS SAME AREA
0.005 x 0.005 in
(2) CURVE 2 21 ELEMENTS 0.003 x 0.005 in
21 ELEMENTS 0.007 x 0.005 in
(3) SERIES R=10 Ω

Figure 18.   Stagger-tuning effect due
to variation in capacitance.

fabricated in this project. This effect is enhanced in shorter delay lines and minimized with longer delays; the coupling capacitance is an inverse function of the geometrical length of the delay rods.
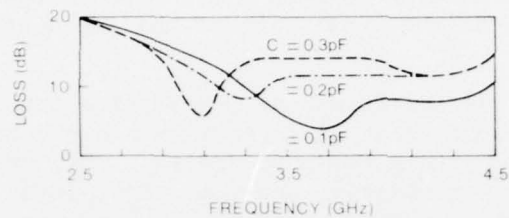
NOTES (1) EXPERIMENTAL VALUE ZnO THICKNESS = 0.25 μm
(2) CONTACT RESISTANCE SIMULATED BY SERIES R = 100 Ω

Figure 19. Effect of variation of feedthrough
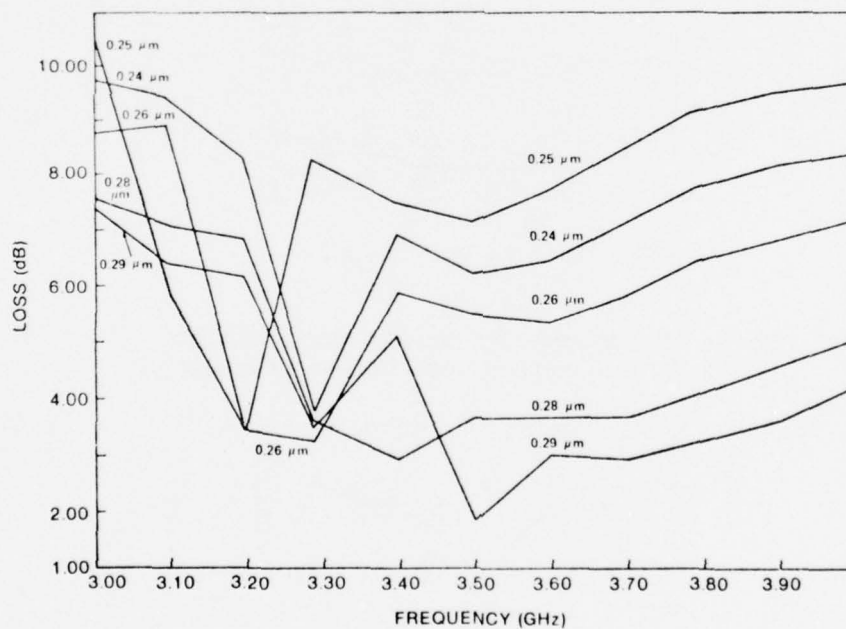capacitance on loss.

Figure 20. Feedthrough loss versus ZnO thickness.

24

6.2 Environmental Tests

Temperature tests were conducted in a Statham chamber. Four unmounted, but completed, units were kept at 80° ± 2°C for 5014 hr. The units were periodically removed from the test chamber and allowed to cool to room temperature. Tests of insertion loss were carried out, and the units were returned to the test chamber. The total elapsed time of removal was about 3 hr for each electrical test. The change in insertion loss was ΔI.L. = +2 dB.

From the total accumulated hours, τ = 5014 hr, in the test chamber without failure, one can predict a lower limit for the mean time between failure (MTBF). By the chi-square test formula,[6]

$$MTBF = \frac{2\tau}{\chi^2(P, \ 2r + 2)} \ ,$$

where P equals unity minus the fractional confidence level (CL), r equals the number of failures, and χ^2 is a statistical function of P and (2r + 2) evaluated from tables in any statistics handbook. Since r = 1 (and 2r + 2 = 4) for some time $>\tau$, this lower limit is given by

$$MTBF > \frac{2\tau}{\chi^2(P, \ 4)}$$

for values of P = 1 − CL. The results are shown in tabular form for several values of confidence level:

Confidence level (%)	$\chi^2(P, \ 4)$	MTBF (hr)
99	13.277	755
90	7.779	1289
80	5.989	1794
70	4.878	2056
50	3.357	2978

6.3 Air-Gun Tests

Mechanical tests were conducted with a 6-in. (21.24-cm) air gun. Tests were carried out at an average of 12,500 g, applied over 1 ms and performed at the Motorola Corp., Phoenix, AZ. Very short

---

[6]W. G. Ireson, *Reliability Handbook*, McGraw-Hill Book Co., New York (1966), 7.

duration peaks to about 15 kg also can be expected to occur during 1 ms. Performance remained unchanged within the range of measurement repeatability.

This test is conducted by firing into a marine plywood target ("mitigator"). Measurements of the initial length and crushed length give the stopping distance. An average acceleration is calculated and compared with high-speed streak photographs taken to determine the acceleration profile. A forecast of extreme gun ruggedness can be made, based on air-gun experience with units having similar construction features (a thin metallic film and ZnO on quartz rods) which survived tests of 76,000 g.

7. CONCLUSIONS AND RECOMMENDATIONS

This project demonstrated production techniques that can produce delay lines using a self-tuned array of microwave acoustic transducers. Two fabrication techniques were demonstrated, plus a third which combined elements of the first two. The new delay lines are physically smaller because of the absence of matching pads, lighter in weight, and highly shock resistant. Assembly requires fewer steps than previous devices, the most beneficial change being elimination of the adjustment needed for external tuning. The lower cost, smaller size, and lower weight now make possible a number of fuze and radar applications not seriously considered earlier. It is recommended that this useful technology be introduced into industry as rapidly as possible. Complete information is available for translation into a mass-production facility.

LITERATURE CITED

(1) R. W. Weinert and J. de Klerk, A Thin-Film Mosaic Transducer for Bulk Waves, IEEE Trans. Sonics Ultrason., SU-19 (July 1972), 354.

(2) T. Reeder and D. Winslow, Characteristics of Microwave Acoustic Transducers for Volume Wave Excitation, IEEE Trans. Microwave Theory Tech., MMT-17, No. 11 (November 1969), 932.

(3) S. Lieberman, Matched Delay Lines with Solderable Transducer Electrodes, U.S. Patent 3,688,222 (29 August 1972).

(4) S. Lieberman, A Rugged Microwave Acoustic Delay Line with Integral Matching, Harry Diamond Laboratories TR-1738 (February 1976).

(5) S. Lieberman, A Matched MIC Delay Line Transducer Using a Series Array, Proc. 1974 IEEE International Solid-State Circuits Conference (1974), 100-101, 235.

(6) W. G. Ireson, Reliability Handbook, McGraw-Hill Book Co., New York (1966), 7.

SELECTED BIBLIOGRAPHY

Adler, E. L., and Fahmy, A. H., Structure and Properties of RF Sputtered ZnO Transducers, IEEE Trans. Sonics Ultrason., SU-19 (July 1972), 346-349.

Berlincourt, D. A., Curran, D. R., and Jaffe, H., in Physical Acoustics, ed. by W. P. Mason, Vol. 1A, Academic Press, New York (1964), 233-242.

Brockelsby, C. F., et al, Ultrasonic Delay Lines, Iliffe Books, Ltd., London (1963), 240-241.

Foster, N. F., et al, IEEE Trans. Sonics Ultrason., SU-15 (1968), 28.

Griffin, J., Evaluation of Microwave Ultrasonic Delay Lines, Harry Diamond Laboratories TR-1441 (May 1969).

Hopp, T. H., Computer-Aided Design of Bulk Microwave Acoustic Delay Lines, Harry Diamond Laboratories TR-1676 (December 1974).

Larson, T., and Finnley, M., Properties of RF Sputtered Zinc Oxide Thin Films for Microwave Acoustic Devices, Naval Research Laboratories Report 7737 (May 1974).

Lieberman, S., Matched MIC Delay Line Transducer Using a Series Array, U.S. Patent 3,893,048 (1 July 1975).

Malbon, R. M., Acoustic Generation with Reactively Deposited Piezoelectric Thin Films, Ph.D. Dissertation, Stanford University (1969). Xerox University Microfilms, Ann Arbor, MI, Accession No. 69-13,984.

Mason, W. P., Physical Acoustics and the Properties of Solids, Van Nostrand Reinhold Co., Princeton, NJ (1958).

Reeder, T. M., and Winslow, D. K., Characteristics of Microwave Acoustic Transducers for Volume Wave Excitation, IEEE Trans. Microwave Theory Tech., MTT-17 (November 1969), 927-941.

Reggia, F., Generation and Propagation of Hypersonic Waves and Their Applications to Microwave Frequencies, Harry Diamond Laboratories TR-1538 (May 1971).

Reggia, F., and Mak, Ting, Electroacoustic Delay Lines for Microwave Frequencies, Harry Diamond Laboratories TR-1382 (March 1968).

APPENDIX A.--PROCESSING TECHNIQUES

FIGURES

APPENDIX A

FIGURES (CONT'D)

A-1. PRELIMINARY COMMENT

The delay line device shown in figure A-1 was fabricated by the steps presented here, which are those followed during the concluding months of the Materials, Methods, and Techniques Effort of the U.S. Army Armament Command. The initial method was restricted to the photolithographic process. The entire sequence of art work and photomask fabrication was carried out within the Harry Diamond Laboratories (HDL).
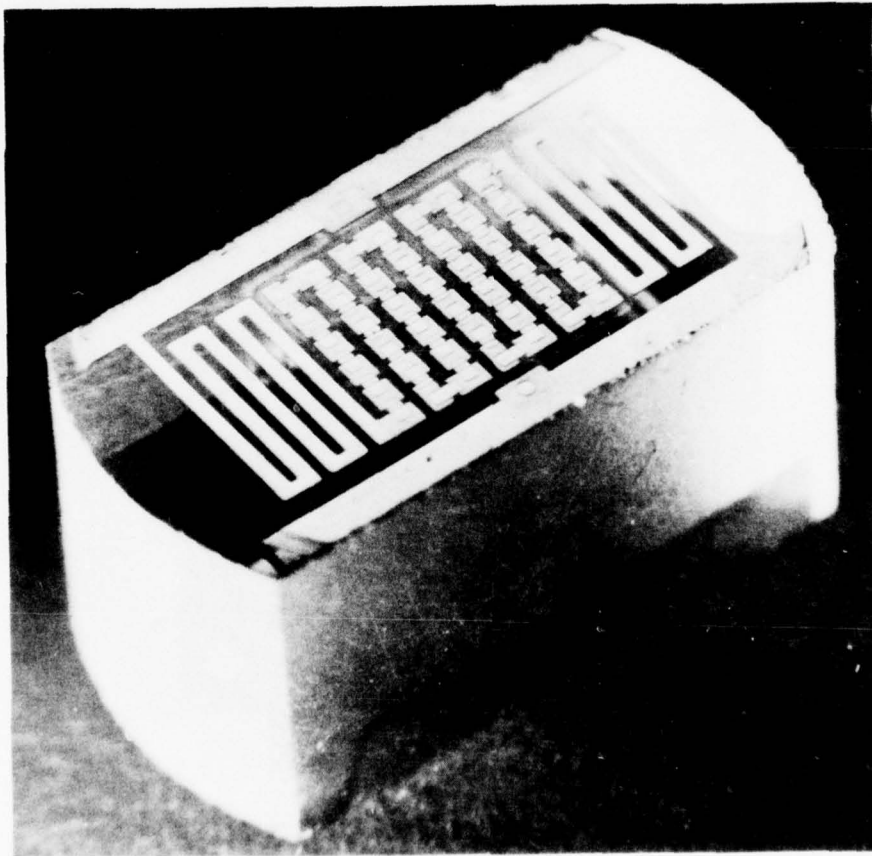

413-75

Figure A-1. Example of completed unit (final design).

APPENDIX A

A second approach used fine-line, stainless steel, metal masks.
Master patterns for these were made at HDL, and these were then
furnished to the Buckbee-Mears Co., St. Paul, MN, who fabricated them
(fig. A-2, A-3). The all-metal mask approach was initially thought to
be attractive since it eliminated the wet chemistry required in handling
photoresist. However, it did prove somewhat difficult during the ZnO
deposition step. This difficulty resulted from the present state of the
art in fabricating fine-line metal masks since the pattern spacing
required for the present design limited the thickness of the mask.
These thin masks also proved difficult to keep consistently in close
contact with the substrate during deposition, and this inconsistency
tended to allow diffusion of sputtered ZnO under the mask. As a result,
some areas had poor deposition.
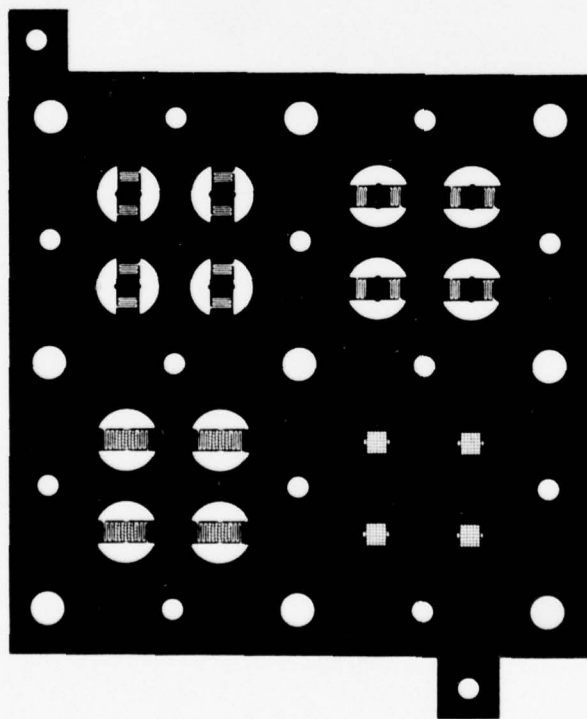
230-77

Figure A-2. Metal mask.
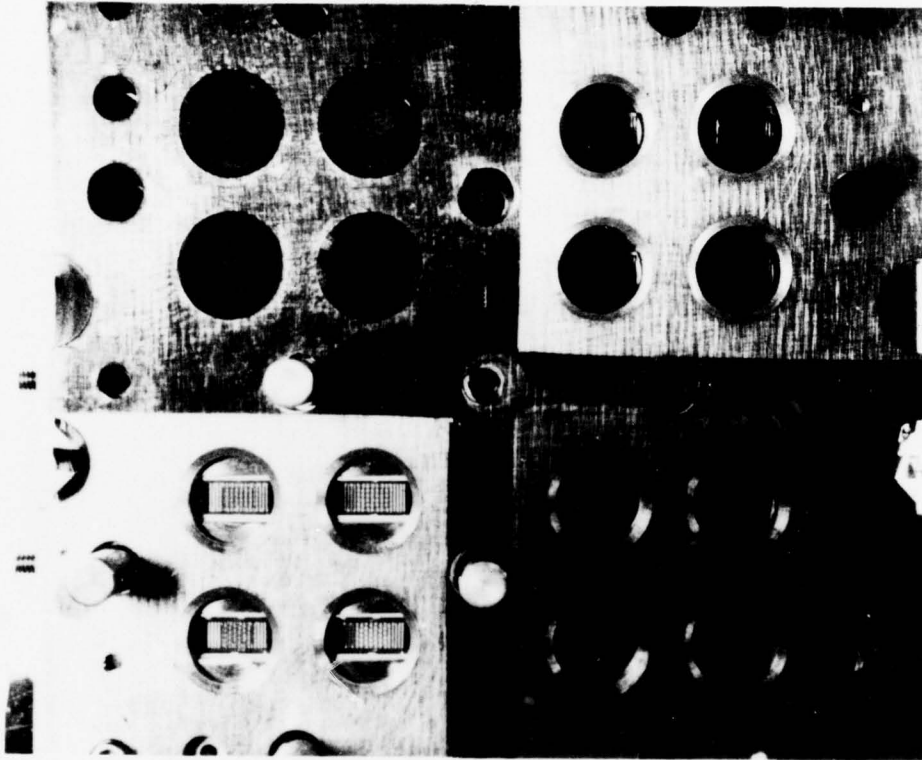
079-75

Figure A-3. Metal mask and fixture.

The final method, described here, was a combination of the above two earlier ones. Photomasks were used for both the ground pattern metallization and the ZnO deposition step, and a metal mask was used for the top electrode metallization only. A description of the processing steps now follows. The transducers were fabricated on rectangular, polished quartz rods since this configuration best suited our previously fabricated test fixture, and a possible application which stressed minimum device size was needed. The techniques followed would naturally be valid for a circular cross-section rod, also.

A-2. PROCESS

A-2.1 <u>Step 1--Crystal Preparation: Lapping Crystals to Size</u>

Synthetically grown crystal quartz, 0.250-in. (0.635-cm) diameter circular rods, Z-axis oriented and polished, are lapped to a rectangular configuration. These rods are ground approximately 20 at a time with two machined brass lapping fixtures, one of which is shown in figure A-4. With diamond abrasive and by grinding techniques,
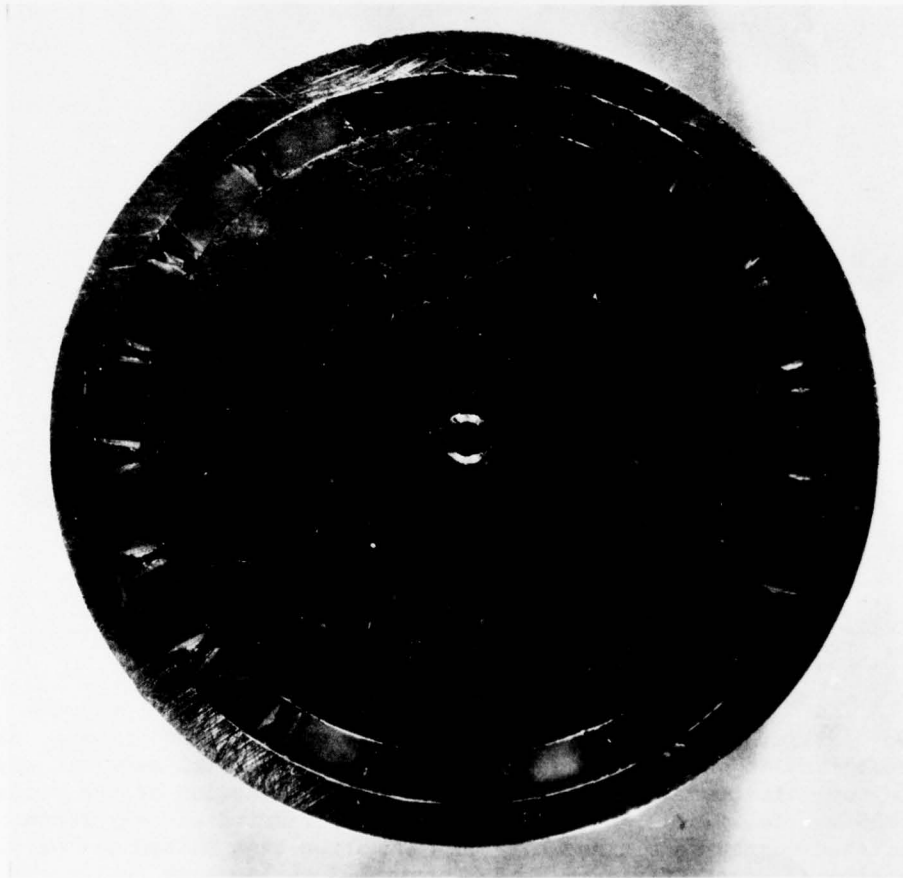
100-75

Figure A-4. Brass lapping fixture, with 19 crystals in position.

dimensions of 0.125 × 0.250 in. (0.318 × 0.635 cm) are successfully
achieved, with final tolerances being held to within a few ten
thousandths of an inch in all measurements.

After several successive stages of lapping are completed, the
quartz rods are removed from the lapping fixture with heat, and the
remnants of bonding stick cement are dissolved with methanol. Then they
are degreased and thoroughly, but gently, scrubbed with a swab and
finally soaked for 1 hr in a specially prepared chemical cleaning
solution.

A-2.2 Step 2--Cleaning

The cleaning solution prepared and used consists of three
parts H_2SO_4, one part H_2O_2, and one part distilled water. Each rod is
soaked in its own spherical, custom-fabricated, glass container; this
technique avoids rod damage from chipping or scratching of highly
polished surfaces (fig. A-5). Rods are stored in a suitable container
in a dust- ee area until insertion in the evaporation system.
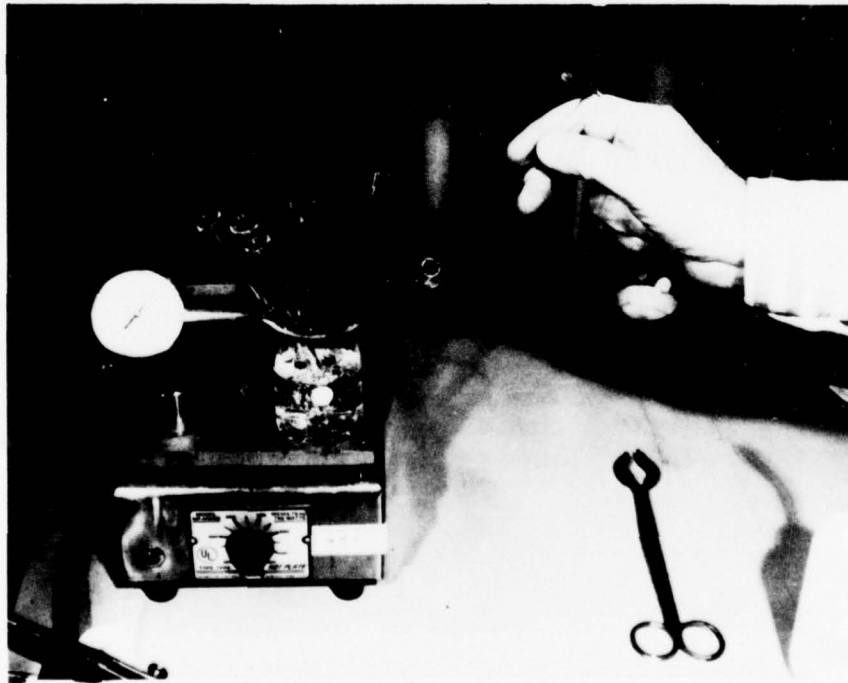
Figure A-5. Rod cleaning technique, showing individual
glass containers.

A-2.3 Step 3--Ground Pattern Evaporation

Chromium and gold layers are evaporated over the entire upper and lower surfaces of polished crystal quartz rods. These are held securely in a suitable fixture having a built-in flip-over device for opposite side metallization during the same run. No mask is used in this step.

a. Install prepared crystals in the rod fixture and insert them in the evaporation system shown in figure A-6.
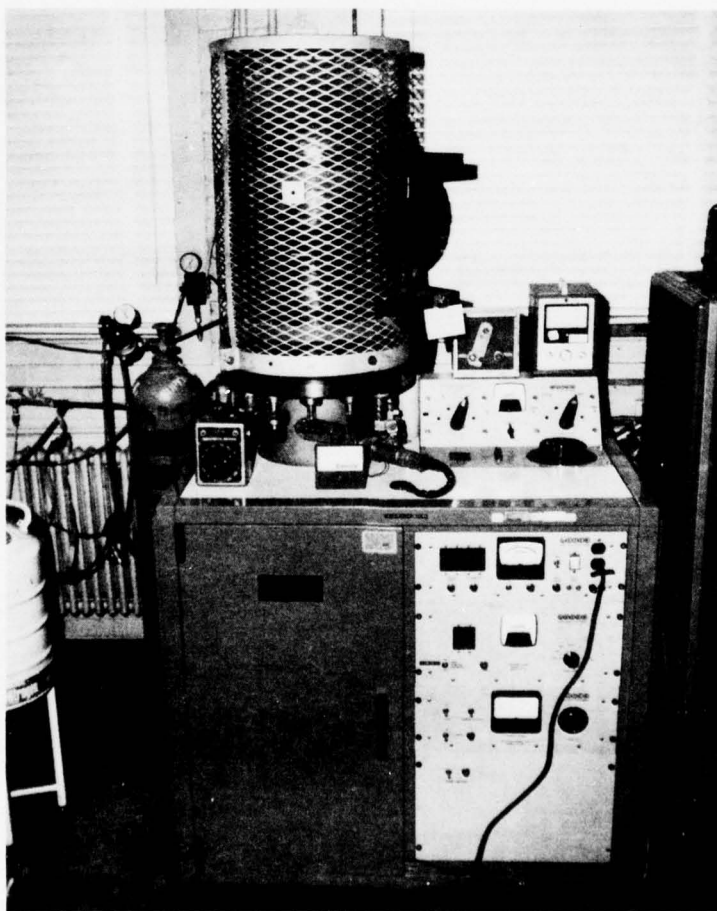
   b. Install a cleaned, pure-chrome pellet and two gold sources
in the tungsten coil filaments visible in figure A-7.
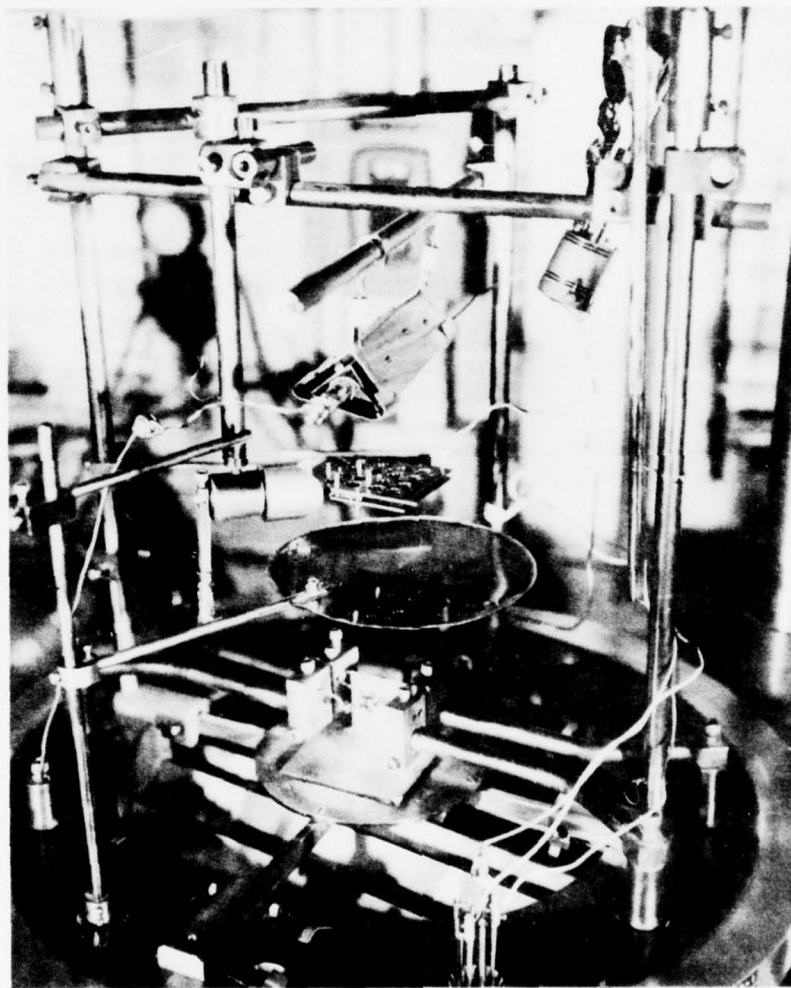
A79-74

Figure A-7. Evaporation system; from top: substrate
            heater, flip-over rod fixture, shutter,
            and tungsten filaments.

37

c. Mount a sample evaporation microscope slide on the shutter.

d. Check the water flow on the Sloan thickness-monitor sensor.

e. Start the evaporation vacuum system pump-down stage.

f. Turn on the substrate heater after 1/2 hr, and slowly increase the Variac setting to 200°C (75 to 80 V). The substrate heater is of the radiant type consisting of a sealed quartz lamp.

g. After the overnight pump down (or equivalent time) at 200°C, check the pressure reading. (It should be 1×10^{-6} mm Hg or lower.)

h. Check each item on the checklist and select the proper electrical connections in the control box.

i. Before actual evaporation of metals (chromium and gold), outgas all sources and filaments thoroughly with the shutter in a closed position.

j. Evaporate some evaporant material on a closed shutter prior to opening the material to the heated substrate to reduce the chances of contamination of metallized layers.

k. Evaporate 2 to 4 μm of chromium in a few seconds to 25 s. Monitor the thickness on a Sloan gauge (crystal quartz oscillator).

l. Evaporate 7 μm of gold on top of the chromium layer.

m. Flip the evaporation fixture over 180 deg using the vacuum feed-through flip-over device provided, and evaporate the chromium and gold on the second side.

n. After completing the evaporation run, cool the substrate for 1 hr and remove the fixture holding the rod from the vacuum system for further steps. This completes the evaporation step for the ground electrode.

A-2.4 Step 4--Application of Photoresist

These procedures pertain to photoresist equipment shown in figure A-8.

477-74

Figure A-8. Photoresist spinner.

a. Turn on the power and pump vacuum lines.

b. Check that the dry nitrogen tank is on.

c. Turn the K-square photoresist spinner toggle switch down to the K-square position and then back it up to neutral. This switch is mounted on the right leg of the alignment microscope bench.

d. Check that all switches on the K-square spinner unit are at the on position, such as power, vacuum, and emergency stop.

e. Swab the brass crystal holding fixture with acetone, and blow the fixture dry.

f. Set the spinner timer for 35 s at 6000 rpm.

39

g. Insert the crystal rod into the fixture first side up using tweezers, and gently tighten the two small set screws.

h. Blow the mounted crystal surface dry with clean tank nitrogen.

i. Use a small-bore medicine dropper or glass syringe to apply 2 drops of GAF PR-425 positive-working resist while spinning the crystal at 6000 rpm.

j. Remove the crystal, and place it in a clean, covered aluminum dish. Be careful not to disturb or touch the resist-coated surface.

k. Bake the first side (top) at 75° to 80°C for 20 min in a clean air oven.

l. Repeat the photoresist coating procedure on side two.

m. After coating side two, perform the final bake at 75° to 80°C for 1 hr.

n. Remove and store the crystal in a clean container.

The photoresist surfaces are unexposed and should be kept in a dark container free from dust and normal room light.

A-2.5 Step 5--Ground Electrodes: Alignment and Exposure

a. Use the special hand-held alignment fixture shown in figure A-9.

b. Check the fixture for accurate parallel alignment of the top and bottom contact photomasks using the contour projector (shadowgraph).

c. Insert a single metallized, crystal quartz rod in the brass alignment fixture, and return the vertical sliding top mask to contact the rod; lock the thumb screw readies on both sides for the first photoresist exposure step.

d. Expose each side separately to the ultraviolet light source for 25 s; by merely inverting the hand fixture without removing or disturbing the crystal's position, expose the second side.
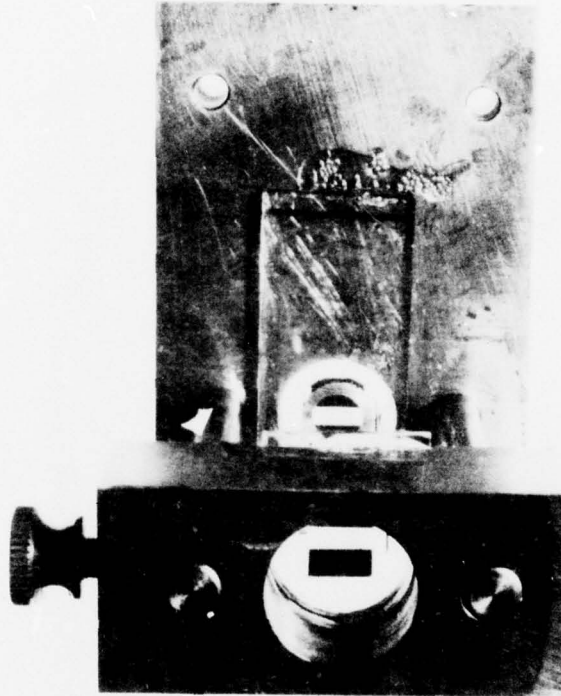
441-74

Figure A-9. Alignment fixture used for ground
electrode pattern.

        e. Two contact photomasks which are permanently mounted in
this hand-held fixture generate these three major patterns on each side
of the crystal quartz rod: (1) a ground electrode for each of 42
transducers, (2) two series inductors, and (3) two large contact areas.
An enlarged view of one of the masks is shown in figure A-10 (p 42).

A-2.6 Step 6--Development of Photoresist

        Caution: Keep the exposed photoresist in the dark until it
is developed and etched.

        a. Use positive working photoresist developer GAF D-014 as
supplied from the vendor.
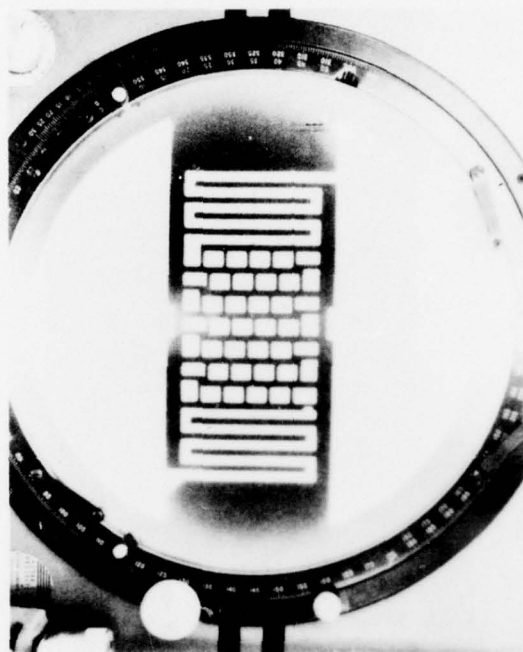
434-74(A)

Figure A-10. Enlarged view of ground electrode mask
as seen in contour projector.

b. Pour the developer solution into a separate container, and
place this in a room-temperature ultrasonic bath as shown in figure A-5.

c. Hold the container with tweezers, and insert the crystal
in the developer solution for 1 min.

d. Transfer the crystal to a clean water container, and hold
it for 30 s.

e. Rinse the container in running distilled water for 1 min.

f. Blow it dry with clean tank nitrogen.

A-2.7 Step 7--Etching Ground Pattern (Chromium and Gold)

a. Mix the gold etch preparation of 100 ml of deionized water, 100 g of KI, and 4 g of iodine.

b. Soak the crystal in the gold etch solution for 1 min in an ultrasonic bath at room temperature.

c. Rinse the crystal in running distilled water for 1 min or more.

d. Mix the chromium etch preparation of 0.95 liters of deionized water, 43 cm^3 of 70 to 72 percent H_2ClO_3, and 170 g of CeNOH.

e. Soak the crystal in the chromium etch solution for 1 min.

f. Rinse the crystal in distilled water, blow it dry with nitrogen, and inspect it.

A-2.8 Step 8--Removal of Photoresist

All remaining photoresist residues following completion of the chromium and gold etching steps must be removed before the sputtering of a ZnO layer.

a. Spray or soak the rod in clean, warm acetone for approximately 5 min.

b. Rinse the rod in running distilled water for 1 to 2 min.

c. Swab or soak the rod in GAF S-050 photoresist stripper solution for several minutes at room temperature.

d. Rinse the rod in running distilled water for 1 to 2 min.

e. Blow the rod dry with clean tank nitrogen.

f. Inspect the rod under a microscope for any trace of remaining photoresist. If any remains, increase the length of time that the rod is in acetone or stripper, or it may be necessary to swab it gently during either the acetone or the stripper stage. Use a final water rinse, and blow the rod dry with nitrogen.

A-2.9 Step 9--Sputtering ZnO Parameters Summarized

This procedure is used in the HDL facility shown in figures A-11 and A-12.
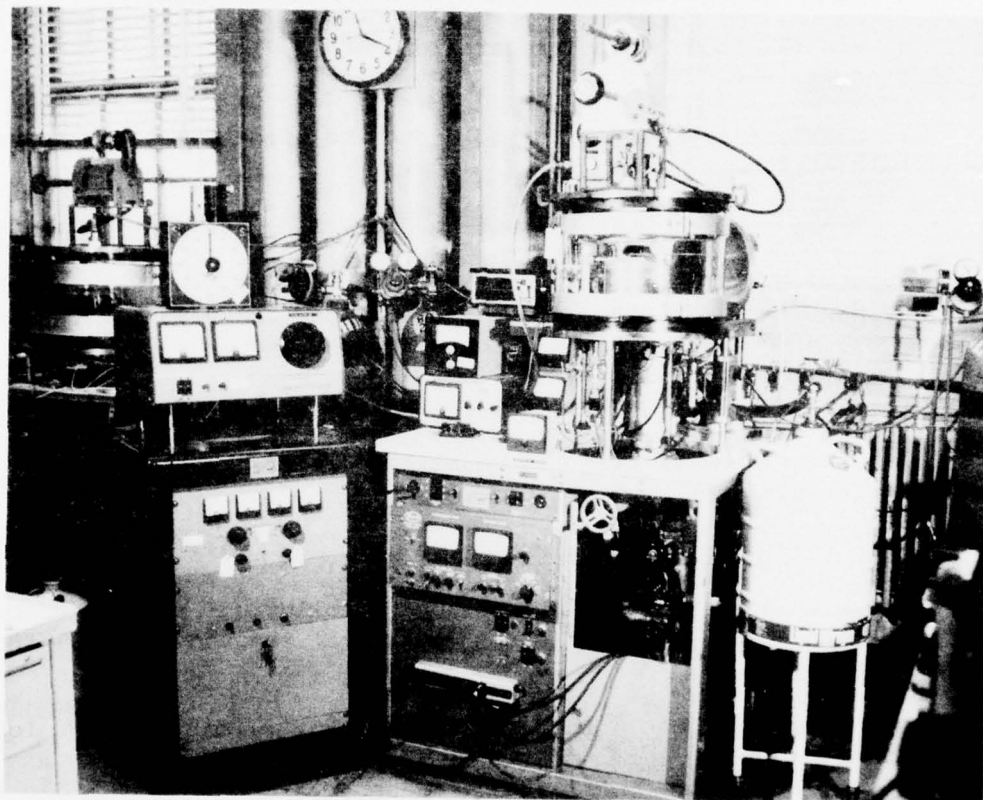
482-74

Figure A-11. Sputtering facility.

        a. For the rf generator, set "tune" at 30, "load" at 186, and "power" at 300 W. Match for a constant 300 W and minimum reflected power.

        b. Set argon and oxygen pressures at 10 psi (68.94 kPa).

        c. Set the gas pressure of the mixture in the system at 20 μm on the Pirani gauge (50-μm scale).

        d. Allow a 5-min rf generator warm-up prior to initial sputtering. Use a Tesla coil for ignition if it is needed.

        e. Maintain a 1/2-in. (1.27-cm) dark space.

44
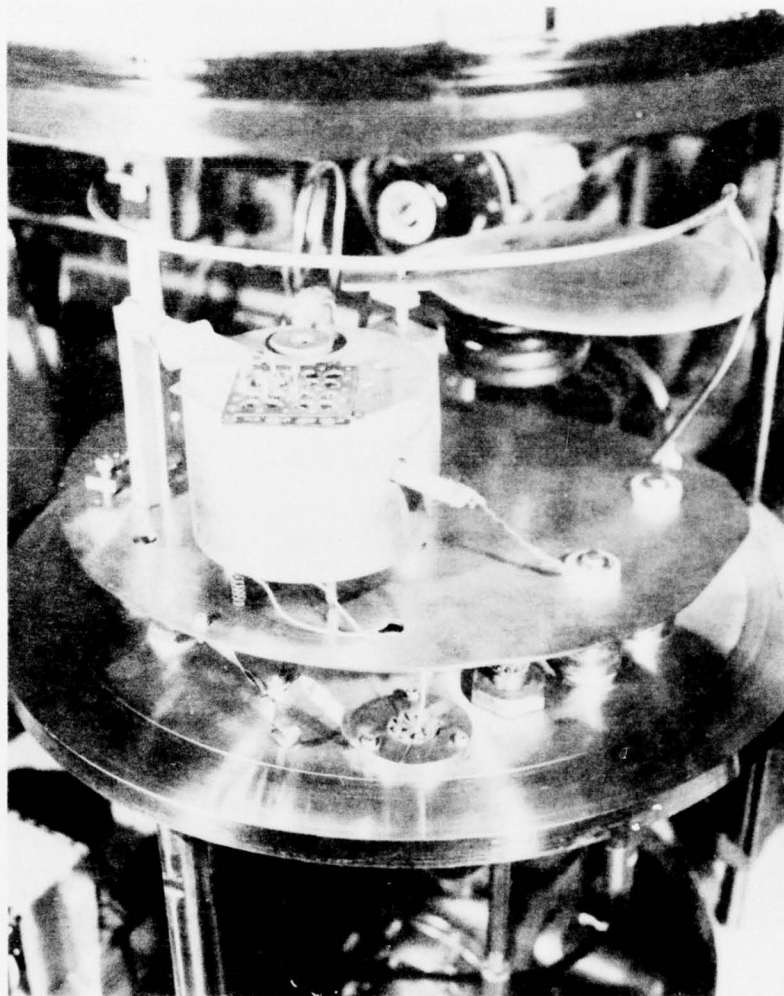
478-74

Figure A-12. Sputtering module with rod fixture and substrate
heater.

    f. Presputter the ZnO for 1 hr with a closed shutter for each
side of the rod.

    g. Keep the initial plate current at 0.5 A.

    h. Hold the substrate at 100° to 120°C throughout the
complete ZnO sputtering process.

i. Continue the actual ZnO deposition for approximately 15 min per side, depending on the rate of deposit indicated on the Inficon digital thickness monitor used for this work.

j. Extinguish the rf discharge during the flip-over process from the first side of the rod to the second side to improve the quality of the ZnO. During some of the earlier ZnO sputtering runs, it was observed that when flip-over of the substrate was initiated, which required the removal of the crystal holder from the plasma and back, often arcing was noticed. The arcing could possibly have a severe degrading effect upon the ZnO sputtered layer. Extinguishing the rf discharge during this stage of the transfer to the second side of the substrate eliminated the arcing, and in so doing there is evidence of improved quality transducer characteristics.

A-2.10   Step 10--Second and Final Photoresist Step

This step follows the sputtering of ZnO entirely on both sides of a delay rod. The details are the same as in step 4.

a. Keep the rods clean and thoroughly dry for application of the photoresist. Store the rods in a clean container after their removal from the vacuum system.

b. Apply the photoresist, GAF PR-425.

c. Prebake the photoresist at 75° to 80°C for 20 min.

d. Postbake the photoresist at 75° to 80°C for 60 min.

e. Store the rods in a clean, dry area and do not expose them to room light until the photoresist is ready for developing.

A-2.11   Step 11--Mask Alignment and Exposure

a. The photomask shown in figure A-13 confines the ZnO piezoelectric layer to areas on top of each of 42 ground pattern electrodes.

b. Using the alignment microscope bench and vacuum chuck shown in figure A-14, contact both sides and then expose them for 25 s to an ultraviolet light source.
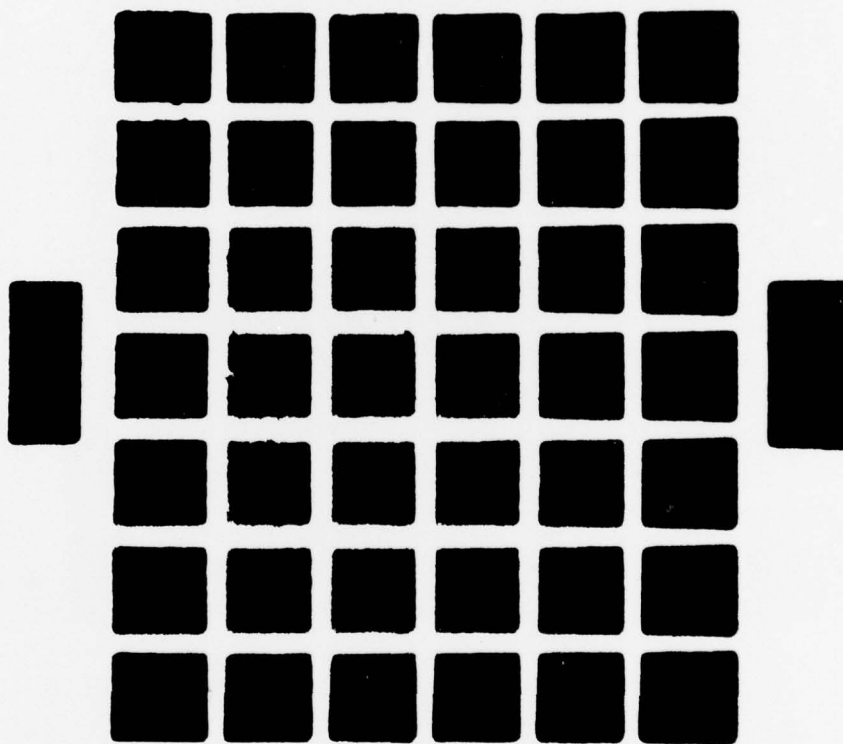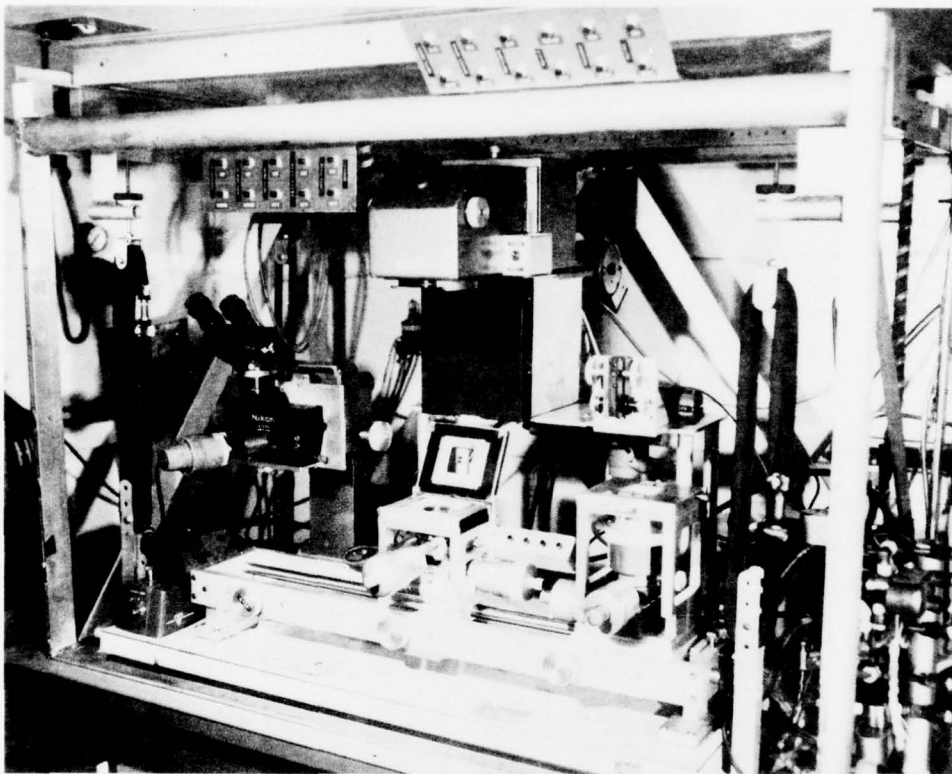
0396-77

Figure A-13. Photomask for deposition of zinc oxide.

APPENDIX A

484-74

Figure A-14. Alignment microscope bench with vacuum chuck
and ultraviolet light source.

A-2.12   Step 12--Development of Photoresist

Follow the details in step 6 for development of the photoresist.

a. Develop the photoresist for 1 min with GAF D-014.

b. Rinse the rods with distilled water.

A-2.13   Step 13--Etching ZnO Sputtered Layer

Remove the ZnO selectively from areas previously defined by the use of masks, using straight H_3PO_4 for 10 s, with a final 2-min distilled water rinse.

Figure A-5. Rod cleaning technique, showing individual
            glass containers.

35

APPENDIX A

       After etching, leave the ZnO covering each of the ground
electrodes, but leave a small area 0.002 in. (0.508 cm) wide uncovered
for the final gold contact to be completed in the next and final
evaporation.

A-2.14   Step 14--Top Electrode Metallization

       The object of this last step is to create a set of
metallic contacts between each of the 42 transducers and thus establish
a series array of transducers.   A thin (0.001 in.--0.0025 cm thick)
stainless steel mask is used to define the top electrode pattern, shown
enlarged in figure A-15.
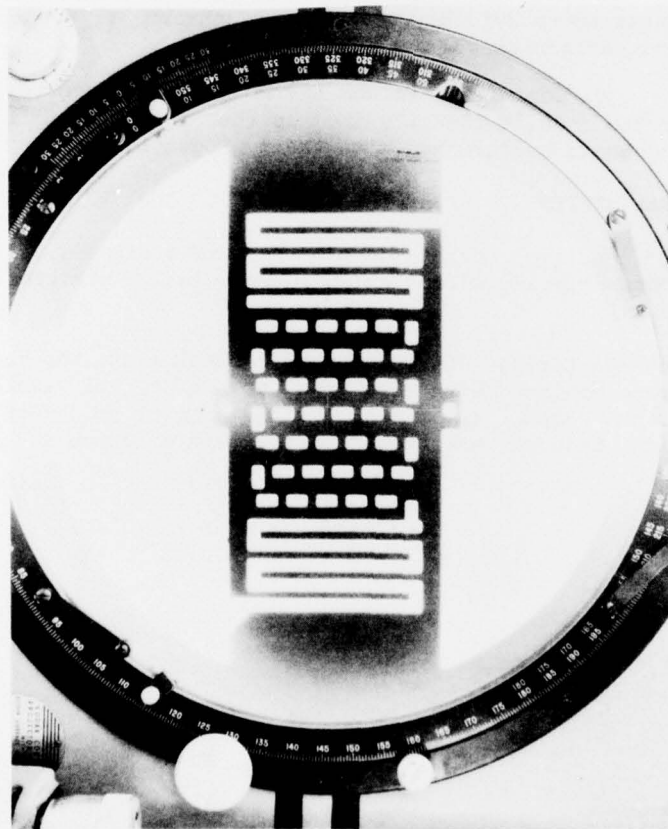
434-74C

Figure A-15. Top electrode metal mask, shown in contour
             projector.

a. Position a separate mask over each end of an individual quartz rod.

b. Using precise registration indicators, align the masks microscopically in the laboratory to conform to the already existing ground metallization and ZnO patterns.

c. Insert the fixture into the vacuum evaporator (fig. A-7), and deposit chromium and gold through the masks. Thicknesses are equivalent to those of the original ground-pattern evaporated metal layers (10 μm). A flip-over feature allows both sides to be metallized in a single evaporation run. Deposit a very thin layer of chrome to enhance the adherence of the gold to those portions of crystal quartz not previously covered by chrome in evaporation of the first ground-pattern step.

d. Cool the vacuum system for 1 hr, remove the fixture, and number the rods to identify them in the future and to facilitate correlating their performance with their processing history.

A-3 GENERAL STATEMENTS REGARDING EVAPORATION AND SPUTTERING

Avoid negative resist developers and strippers, since they have a severe deteriorating effect on ZnO, especially strippers containing H_2SO_4.

During sputtering, through or on a metal mask, the mask must be in good intimate contact with the rod or wafer, to avoid sputtering underneath the edges. In our situation, snap rings tended to alleviate the problem. Thicker masks would be the best solution.

DISTRIBUTION

DEFENSE DOCUMENTATION CENTER
CAMERON STATION, BUILDING 5
ALEXANDRIA, VA 22314
  ATTN DDC-TCA (12 COPIES)

COMMANDER
USA RSCH & STD GP (EUR)
BOX 65
FPO NEW YORK 09510
  ATTN LTC JAMES M. KENNEDY, JR.
       CHIEF, PHYSICS & MATH BRANCH

COMMANDER
US ARMY MATERIEL DEVELOPMENT
 & READINESS COMMAND
5001 EISENHOWER AVENUE
ALEXANDRIA, VA 22333
  ATTN DRXAM-TL, HQ TECH LIBRARY

COMMANDER
US ARMY ARMAMENT MATERIEL
 READINESS COMMAND
ROCK ISLAND ARSENAL
ROCK ISLAND, IL 61201
  ATTN DRSAR-ASF, FUZE &
       MUNITIONS SPT DIV

COMMANDER
USA MISSILE & MUNITIONS CENTER & SCHOOL
REDSTONE ARSENAL, AL 35809
  ATTN ATSK-CTD-F

HARRY DIAMOND LABORATORIES
  ATTN LOWREY, AUSTIN, III, COL, COMMANDER/
       FLYER, I.N./LANDIS, P.E./
       SOMMER, H./OSWALD, R. B.
  ATTN CARTER, W.W., DR., TECHNICAL
       DIRECTOR/MARCUS, S.M.
  ATTN KIMMEL, S., PAO
  ATTN CHIEF, 0021
  ATTN CHIEF, 0022
  ATTN CHIEF, LAB 100
  ATTN CHIEF, LAB 200
  ATTN CHIEF, LAB 300
  ATTN CHIEF, LAB 400
  ATTN CHIEF, LAB 500
  ATTN CHIEF, LAB 600
  ATTN CHIEF, DIV 700
  ATTN CHIEF, DIV 800
  ATTN CHIEF, LAB 900
  ATTN CHIEF, LAB 1000
  ATTN RECORD COPY, BR 041
  ATTN HDL LIBRARY (5 COPIES)
  ATTN CHAIRMAN, EDITORIAL COMMITTEE
  ATTN CHIEF, 047
  ATTN TECH REPORTS, 013
  ATTN PATENT LAW BRANCH, 071
  ATTN GIDEP OFFICE, 741
  ATTN LANHAM, C., 0021
  ATTN LIEBERMAN, S., 950 (5 COPIES)
  ATTN WASILIK, J., 210
  ATTN BLOMQUIST, T., 950
  ATTN MEYER, O., 230
  ATTN CULLINANE, J., 620
  ATTN MCDONALD, D., 950
  ATTN REDDAN, M., 950 (5 COPIES)

DAT
FILM